Estimation of Parameters of a Three-phase Induction Motor Based on Experimental Data and Modeling Results Based on SINDYc

Spodoba M.O., Spodoba O.O., Kovalchuk S.I.
National University of Life and Environmental Sciences of Ukraine,
Kyiv, Ukraine

Abstract. The aim of the work is to study the dynamic behavior of induction motors and estimate key electromechanical parameters using the SINDYc method in conditions where only the results of no-load and short-circuit tests and a dataset with reference data of various three-phase induction motors of the AIR series are available. To achieve this goal, general physics methods, three-dimensional modeling, processing and visualization of results in the Wolfram Mathematica program were used. The working hypothesis of the research is to investigate the possibilities of using SINDYc to estimate the dynamics of key electromechanical parameters of three-phase induction motors, subject to limited input data and the availability of reference data of various three-phase induction motors of the AIR series. The most important result is the combination of parameters obtained from experiments of no-load and short-circuit of a three-phase asynchronous motor with a dataset of characteristics of various motors of the corresponding series, and unknown quantities are found using the developed mathematical model and the use of calculation relations given in this work. The significance of the research results obtained in the work lies in the fact that based on the developed method, it is possible to analyze the dynamic behavior of asynchronous motors and evaluate the dynamics of key electromechanical parameters of an electric motor using the SINDYc method in conditions when only the results of no-load and short-circuit tests are available. The results of the analysis of the sparsity of the SINDYc model showed that in the studied range of threshold values, the accuracy on the test sample practically does not change, while the number of active terms in the equations changes moderately.
Keywords: SINDYc method, asynchronous electric motor, electromagnetic moment, rotor, modeling.

DOI: https://doi.org/10.52254/1857-0070.2026.1-69.14
UDC: 620.9.004.18

Estimarea parametrilor unui motor cu inducție trifazat pe baza datelor experimentale și a rezultatelor modelării bazate pe SINDYc

Spodoba M.O., Spodoba O.O., Kovaliciuk S.I.
Universitatea Națională a resurselor biologice li utilizarea naturii a Ucrainei, Kyiv, Ucraina

Rezumat. Scopul lucrării este de a studia comportamentul dinamic al motoarelor asincrone și evaluarea parametrilor electromecanici cheie utilizând metoda SINDYc în condiții în care sunt disponibile doar rezultatele testelor la mers în gol și la scurtcircuit și un set de date cu valori de referință pentru diferite motoare asincrone trifazate din seria AIR. Pentru atingerea obiectivelor, au fost utilizate metode generale a fizicii, modelare tridimensională, procesare și vizualizare a rezultatelor în programul Wolfram Mathematica. Ipoteza de lucru a cercetării este de a investiga posibilitățile de utilizare a SINDYc pentru a estima dinamica parametrilor electromecanici cheie ai motoarelor asincrone trifazate, în condițiile unor date de intrare limitate și a disponibilității datelor de referință ale diferitelor motoare asincrone trifazate din seria AIR. Cel mai important rezultat constă în combinarea parametrilor obținuți din experimentele de mers în gol și în scurtcircuit ale unui motor asincron trifazat cu un set de date cu caracteristicile diferitelor motoare din seria corespunzătoare, iar mărimile necunoscute sunt găsite folosind modelul matematic elaborat și utilizarea relațiilor de calcul prezentate în această lucrare. Semnificația rezultatelor cercetării obținute în lucrare constă în faptul că, pe baza metodei elaborate, este posibilă analiza comportamentului dinamic al motoarelor asincrone și evaluarea dinamicii parametrilor electromecanici cheie ai unui motor electric utilizând metoda SINDYc în condiții în care sunt disponibile doar rezultatele testelor la mers în gol și la scurtcircuit.
Cuvinte-cheie*:* metoda SINDYc, motor electric asincron, cuplu electromagnetic, rotor, modelare.

Оценка параметров трехфазного асинхронного двигателя за экспериментальными данными и расчетом модели на основе SINDYc

Сподоба М.А., Сподоба А.А., Ковальчук С.И.
Национальный университет биоресурсов и природопользования Украины, Киев, Украина

Аннотация. Целью работы является исследование динамического поведения асинхронных двигателей и оценка ключевых электромеханических параметров с использованием метода SINDYc в условиях, когда есть только результаты испытаний холостого хода, короткого замыкания и датасет с эталонными данными различных трехфазных асинхронных двигателей серии АИР. Для достижения поставленных целей использовались общие методы физики, трехмерное моделирование, обработка и визуализация результатов в программе Wolfram Mathematica. Рабочая гипотеза исследований состоит в том, чтобы исследовать возможности применения SINDYc для оценки динамики ключевых электромеханических параметров трехфазных асинхронных двигателей при ограничении исходных данных и наличии эталонных данных различных трехфазных асинхронных двигателей серии АИР. Наиболее важным результатом является сочетание параметров полученных из эксериментов холостого хода и короткого замыкания трехфазного асинхронного двигателя с датасетом характеристик различных двигателей соответствующей серии, а неизвестные величины находятся с помощью разработанной математической модели и использования расчетных соотношений, приведенных в данной работе. Значимость полученных в работе результатов исследований состоит в том, что на основе разработанного метода можно проводить анализ динамического поведения асинхронных двигателей и проведение оценки динамики ключевых электромеханических параметров электрического двигателя методом SINDYc в условиях, когда есть только результаты испытаний холостого хода и короткого замыкания. Результаты анализа разреженности модели SINDYc показали, что в исследованном диапазоне пороговых значений точность на тестовой выборке практически не меняется, в то время как количество активных членов в уравнениях меняется умеренно. Для большинства пороговых значений в интервале 0.01–0.50 было получено практически одинаковый средний уровень погрешности 0.047808, при этом модель содержит около 225 ненулевых членов. В ходе проверки достоверности идентифицированной модели SINDYc была получена стабильная численная симуляция на всем тестовом интервале, что указывает на пригодность найденной системы уравнений как прогностическое приближение динамики.

Ключевые слова: метод SINDYc, асинхронный электрический двигатель, электромагнитный момент, ротор, моделирование.

INTRODUCTION

Asynchronous motors are the most common type of electric machines – they account for about 80% of rotating mechanisms in modern industry in different countries of the world [1]. This is a consequence of the simplicity of design, reliability, low cost and high efficiency of asynchronous motors [2]. One of the main criteria is the availability of a wide range of asynchronous motors with different power characteristics, and their availability on the markets is also an advantage. Asynchronous electric motors have become widespread in renewable energy facilities, namely biogas technologies [3-6].

Ensuring effective fermentation of raw materials in a biogas reactor is achieved by creating the necessary microclimate in the biogas reactor and ensuring a homogeneous substance. For this purpose, various mixing devices are used [7-10], the drives of which are asynchronous electric motors.

The raw materials in the biogas reactor change their physicochemical composition in the process of anaerobic fermentation, which leads to compaction of the sediment and unpredictability of changes in the torque on the electric motor shaft in the initial periods of movement – start-up mode, and steady-state operation modes. Motor overload, beating or jamming of the rotor of an asynchronous electric motor lead to overheating of the electrical windings, destruction of insulation and the appearance of other malfunctions [11-14], which lead to emergency operation of the electric motor and the impossibility of its further operation without repair work.

Under industrial operating conditions, motors age and lose their properties over time [15-19]. Continuous operation involves complex interactions between electromagnetic and mechanical subsystems. These inherent operational factors create constant loads on bearing assemblies and induce vibrations which eventually accelerate the wear of electrical machine elements [20]. This leads to machine failure and disruption of technological processes, which in turn leads to material losses, underproduction, plant downtime, etc.

Traditional physically oriented models, in particular multi-loop equivalent circuits, describe the operation of induction motors well, but their accuracy relies heavily on precise knowledge of

the machine parameters [21]. In industrial scenarios, where exact parameters and varying operating conditions are often unknown or fluctuate, the model's fidelity decreases. Consequently, adapting such models to reflect the actual state of the machine requires continuous parameter identification and additional measurements, which complicates practical implementation [21].

Today, there are many strategies and methods for monitoring the condition of induction motors, including the preventive maintenance approach. This approach is based on continuous monitoring of the performance of induction motors in order to detect faults at the initial stages, all this allows you to plan repair work before critical situations arise that lead to equipment failures [22, 23]. However, this approach requires processing a large amount of experimental data, and continuous control and monitoring, which is an energy-intensive solution.

As a result of the emergence of Industry 5.0 and the rapid development of artificial intelligence, machine learning methods are becoming increasingly common in systems for monitoring and detecting faults in asynchronous motors [1, 24-32]. Classical machine learning techniques, such as Support Vector Machine (SVM) [24], Decision Trees [25], and Artificial Neural Networks [26], and other methods, the description of which is given in more detail in [1, 27-32].

However, these methods are often based on manual and time-consuming processes of selecting and extracting relevant features, which limits their ability to capture complex and nonlinear patterns in induction motor data.

In recent years, data-driven approaches have been developed that allow building model dynamics without a detailed physical description, using time series of experimentally measured data [33, 34]. One of such methods is Sparse Identification of Nonlinear Dynamics with Control (SINDYc) – an algorithm that restores sparse, interpreted nonlinear models of dynamic systems based on experimentally measured data [21, 35-37]. When applied to electric machines, this approach has demonstrated high accuracy in reproducing the dynamics of currents and electromagnetic torque [34, 37].

Also, the capability of SINDYc to evaluate complex electromechanical dynamics has been demonstrated. This is crucial, as the nature of these dynamic processes defines the operational stability and determines the rate of wear for bearings and mechanical rotating parts [35-37]. Most of the work on the application of SINDYc relies on complete data sets that contain not only electrical but also experimentally measured mechanical parameters: torque, angular velocity, winding temperature, etc. Obtaining such data requires conducting long and financially expensive experiments with a developed measurement infrastructure – for example, using encoders to measure speed and loading machines to control torque [34]. This complicates the initial verification of the methods, especially when only standard no-load and short-circuit tests are available. It is possible to supplement the experimental research data by mathematical modeling, which will significantly improve the quality of subsequent calculations.

Failure of the electric drive for mixing raw materials in biogas reactors will lead to negative consequences: loss of raw materials, death of bacterial colonies, cessation of biogas formation. All this leads to significant material and capital costs. Therefore, it is advisable to develop various methods aimed at assessing the dynamics of currents and electromagnetic torque under conditions of limited initial data. This will make it possible to predict the operating mode of the electric motor and use the obtained data to develop automatic control systems for mixing devices with the consumption of the least amount of electrical energy for the corresponding type of raw materials and mixing mode.

This paper proposes an intermediate stage – mathematical modeling of the possibility of using SINDYc to estimate the dynamics of currents and electromagnetic torque under conditions of limited initial data. We combine the parameters obtained from no-load and short-circuit experiments with a dataset of characteristics of various motors, and the missing values are restored through calculated relationships. Thus, a synthetic dataset is formed for training and testing the method. The aim of this paper is to investigate the dynamic behavior of induction motors and to estimate key electromechanical variables using the SINDYc method, relying solely on results from standard tests and reference data from AIR series three-phase induction motors.

RESEARCH METHODOLOGY

The input data for this study include data sets from no-load and locked-rotor induction motor tests, as well as a data set of catalog specifications for standard motors. The measured quantities in

the data set include: phase-to-phase voltage, V; phase-to-phase current, A; total active power of the three-phase network, W.

The averaged line-to-line voltage and line current:

$$U_{line} = \frac{U_{AB} + U_{BC} + U_{CA}}{3} \quad (1)$$

$$I_{avg} = \frac{I_A + I_B + I_C}{3} \quad (2)$$

where U_{line} – average line voltage, V; U_{AB}, U_{BC}, U_{CA} – phase-to-phase voltages, V; I_{avg} – average phase current, A; I_A, I_B, I_C – phase currents, A.

Power factor is computed as:

$$\cos\varphi = \frac{P}{\sqrt{3} \cdot U_{line} \cdot I_{avg}} \quad (3)$$

where $\cos\varphi$ – power factor; P – active power, W.

Assumes star (Y) connection for the test and catalog data. Then:

$$U_{ph} = \frac{U_{line}}{\sqrt{3}} \quad (4)$$

where U_{ph} – phase voltage, V.

$$I_{ph} = I_L \quad (5)$$

where U_{ph} – per-phase RMS voltage, V; I_{ph} – pe-phase RMS current, A.

A first-order no-load per-phase active power model is:

$$P_{0,ph} \approx \frac{U_{ph}^2}{R_c} + P_{f\omega,ph} \quad (6)$$

where $P_{0,ph}$ – no-load per-phase power, W; R_c – core-loss resistance, Ohm; $P_{f\omega,ph}$ – per-phase friction (mechanical loss) power, W.

$$P_{0,ph} = \frac{\left(P_0 - 3I_{ph}^2 R_1\right)}{3} = \frac{P_0}{3} - I_{ph}^2 R_1 \quad (7)$$

where R_1 – preliminary stator resistance, Ohm.

A linear regression is applied:

$$P_{0,ph} \approx a \cdot U_{ph}^2 + b \quad (8)$$

$$R_c \approx \frac{1}{a} \quad (9)$$

$$P_{f\omega,ph} \approx b \quad (10)$$

where a – is regression slope, W/V^2; b – is regression intercept, W.

To estimate the magnetizing reactance, the no-load current is split into core-loss and magnetizing components:

$$I_c = \frac{U_{ph}}{R_c} \quad (11)$$

$$I_m = \sqrt{I_{ph}^2 - I_c^2} \quad (12)$$

$$X_m = \frac{U_{ph}}{I_m} \quad (13)$$

where I_c – is core-loss branch current, A; I_m – is magnetizing current, A; X_m – is magnetizing reactance, Ohm.

For locked-rotor conditions, slip is s=1, and the per-phase input impedance magnitude is approximated by:

$$Z_{sc} = \frac{U_{ph}}{I_{ph}} \quad (14)$$

where Z_{sc} – is per-phase locked-rotor impedance magnitude, Ohm.

The per-phase active power is:

$$P_{sc.ph} = \frac{P_{sc}}{3} \quad (15)$$

where P_{sc} – is total three-phase locked-rotor active power, W.

The equivalent resistance is estimated by:

$$R_{eq} = \frac{P_{sc.ph}}{I_{ph}^2} \quad (16)$$

$$X_{eq} = \sqrt{Z_{sc}^2 - R_{eq}^2} \quad (17)$$

In the classical T-equivalent representation:

$$R_{eq} = R_1 + R_2^{/} \quad (18)$$

$$Z_{eq} = X_1 + X_2^{/} \quad (19)$$

where R_1 – is stator resistance, Ohm; $R_2^{/}$ – is rotor resistance referred to stator, Ohm; X_1 – is stator leakage reactance, Ohm; $X_2^{/}$ – is rotor leakage reactance referred to stator, Ohm.

Model filters out non-physical points using $0 < \cos\varphi \le 1$ and excludes the lowest-voltage regime to reduce noise sensitivity.

Steady-State T-Equivalent Circuit Model (used for inverse fitting). Synchronous speed and slip:

$$\omega_e = 2\pi f \tag{20}$$

where ω_e – is stator angular frequency, rad/s; f – is supply frequency, Hz.

The synchronous speed is:

$$\omega_{sync} = \frac{\omega_e}{2p} \tag{21}$$

$$n_s = \frac{60f}{2p} \tag{22}$$

where p – is number of pole; ω_{sync} – is synchronous angular speed, rad/s; n_s – is synchronous speed, rpm.

Slip is:

$$s = \frac{\omega_{sync} - \omega_m}{\omega_{sync}} \tag{23}$$

where ω_m – is rotor speed, rpm.

Per-phase impedance model:

$$Z_1 = R_1 - jX_1 \tag{24}$$

$$Z_2 = \frac{R_2^{/}}{s} + jX_2^{/} \tag{25}$$

where Z_1 – is stator impedance, Ohm; Z_2 – is rotor referred impedance (slip-dependent), Ohm.

The magnetizing branch impedance is:

$$Z_m = \left(\frac{1}{R_c} + \frac{1}{jX_m}\right)^{-1} \tag{26}$$

where Z_m – is magnetizing branch impedance, Ohm.

The parallel combination of magnetizing and rotor branches:

$$Z_p = \left(\frac{1}{Z_m} + \frac{1}{Z_2}\right)^{-1} \tag{27}$$

$$Z_{in} = Z_1 + Z_p \tag{28}$$

where Z_{in} – is per-phase input impedance, Ohm.

The per-phase current phasor is:

$$I_1 = \frac{U_{ph}}{Z_{in}} \tag{29}$$

where I_1 – is per-phase input current phasor, A.

Power factor is:

$$\cos\varphi = \cos\left(\angle Z_{in}\right) \tag{30}$$

where $\angle Z_{in}$ – is the phase angle of Z_{in}, rad.

Three-phase input power:

$$P_{in} = 3\Re\left\{U_{ph} I_1^*\right\} \tag{31}$$

where $\Re\{\ \}$ – denotes real part; $\left\{U_{ph} I_1^*\right\}$ - denotes complex conjugate; P_{in} – is total input active power, W.

Let the internal (air-gap) voltage be:

$$U_p = U_{ph} - I_1 \cdot Z_1 \tag{32}$$

where U_p – is the per-phase voltage at the parallel node, V.

Rotor branch current:

$$I_2^{/} = \frac{U_{ph}}{Z_2} \tag{33}$$

where $I_2^{/}$ – is rotor current referred to stator, A.

Air-gap power:

$$P_{ag} = 3\left|I_2^{/}\right|^2 \frac{R_2^{/}}{s} \tag{34}$$

where P_{ag} – is air-gap power, W.

Converted electromagnetic power:

$$P_{conv} = P_{ag}\left(1 - s\right) \tag{35}$$

where P_{conv} – is converted mechanical power, W.

Shaft output power is modeled as:

$$P_{out} = \max\left(P_{conv} - P_{f\omega,}\, 0\right) \tag{36}$$

where P_{out} – is shaft output power, W; $P_{f\omega}$ – is mechanical loss power, W.

Efficiency:

$$\eta = \frac{P_{out}}{P_{in}} \tag{37}$$

where η – is efficiency.

Torque:

$$T = \frac{P_{out}}{\omega_m} \tag{38}$$

$$\omega_m = \frac{2\pi n}{60} \tag{39}$$

where T – is shaft torque, Nm; n – is rotor speed, rpm.

Catalog-Constrained Inverse Parameter Fit. For each catalog row (rated values), the model estimates:

For each catalog row (rated values), the model estimates:

$$\theta = \left[R_1, X_1, R_2^{/}, X_2^{/}, X_m, R_c, P_{f\omega}\right] \quad (40)$$

Given catalog measurements:

$$U_{LL,r}, I_{L,r}, \cos\varphi_r, n_r, \eta_r, T_r \quad (41)$$

where r – denotes rated/catalog values.

The inverse problem minimizes a normalized residual vector:

$$\min_{\theta} \left\| r(\theta) \right\|_2^2 \quad (42)$$

With residual components:

$$r(\theta) = \begin{bmatrix} \dfrac{I_L(\theta) - I_{L,r}}{I_{L,r}} \\ \dfrac{\cos\varphi(\theta) - \cos\varphi_r}{\cos\varphi_r} \\ \dfrac{T(\theta) - T_r}{T_r} \\ \dfrac{\eta(\theta) - \eta_r}{\eta_r} \\ \lambda_x \dfrac{X_1 - X_2^{/}}{Z_b} \\ \lambda_r \dfrac{R_1 - R_2^{/}}{Z_b} \end{bmatrix} \quad (43)$$

Where $I_L(\theta), \cos\varphi(\theta), T(\theta), \eta(\theta)$ – are computed by the steady-state model; λ_x, λ_r – are soft-prior weights; Z_b – is a base impedance used for scaling, Ohm.

$$Z_b = \frac{U_{ph,r}}{I_{L,r}} \quad (44)$$

$$U_{ph,r} = \frac{U_{LL,r}}{\sqrt{3}} \quad (45)$$

Multi-start bounded least squares is used to reduce local minima sensitivity.

Matching the unknown motor to catalog candidates. From the unknown motor tests, a feature vector is formed:

$$u = \left[R_c, X_m, R_{eq}, X_{eq}\right] \quad (46)$$

From each catalog inverse fit:

$$c = \left[R_c, X_m, R_{eq}, X_{eq}\right] \quad (47)$$

A log-space weighted distance:

$$d(u,c) = \sqrt{\sum_k \omega_k \left(\log_{10} u_k - \log_{10} c_k\right)^2} \quad (48)$$

where ω_k – are chosen weights; d – is dimensionless.

Additionally, a curve-based score compares predicted and measured no-load/locked-rotor curves using a normalized RMSE. For a quantity:

$$NRMSE(y) = \frac{\sqrt{\dfrac{1}{N}\sum_{i=1}^{N}\left(y_i^{pred} - y_i^{means}\right)^2}}{\sum_{i=1}^{N}\left(y_i^{means}\right)} \quad (49)$$

where N – is the number of data points; y – quantity.

Dynamic αβ induction motor model (time-domain simulation). Reactance-to-inductance conversion. Using the fitted reactances:

$$L_{ls} = \frac{X_1}{\omega_e} \quad (50)$$

$$L_{lr}^{/} = \frac{X_2}{\omega_e} \quad (51)$$

$$L_m = \frac{X_m}{\omega_e} \quad (52)$$

where L_{ls} – is stator leakage inductance, H; $L_{lr}^{/}$ – is rotor leakage inductance referred to stator, H; L_m – is magnetizing inductance, H.

Define:

$$L_s = L_{ls} + L_m \quad (53)$$

$$L_r = L_{lr}^{/} + L_m \quad (54)$$

$$\sigma = 1 - \frac{L_m^2}{L_s L_r} \quad (55)$$

where L_s – is stator inductance, H; L_r – is rotor inductance, H; σ – is leakage factor.

Rotor time constant:

$$\tau_r = \frac{L_r}{R_2^{/}} \quad (56)$$

where τ_r – is rotor time constant, s.

Electrical rotor speed:

$$\omega_{r,e} = 2p\omega_m \quad (57)$$

where $\omega_{r,e}$ – is rotor electrical angular speed, rad/s.

State, inputs, and instantaneous voltages. The state vector is:

$$X = \left[i_{s\alpha}, i_{s\beta}, \psi_{r\alpha}, \psi_{r\beta}, \omega_m\right]^T \quad (58)$$

where $i_{s\alpha}, i_{s\beta}$ – are stator currents in αβ frame, A; $\psi_{r\alpha}, \psi_{r\beta}$ – are rotor flux linkages in αβ frame, Wb.

The input vector is:

$$u = \left[\nu_{s\alpha}, \nu_{s\beta}, T_L\right]^T \quad (59)$$

where $\nu_{s\alpha}, \nu_{s\beta}$ – are instantaneous stator voltages in αβ, V; T_L - is load torque, Nm.

The model generates a sinusoidal αβ voltage with ramped peak amplitude:

$$\nu_{s\alpha}(t) = U_{pk}(t)\cos(\omega_e t) \quad (60)$$

$$\nu_{s\beta}(t) = U_{pk}(t)\sin(\omega_e t) \quad (61)$$

$$U_{pk}(t) = ramp(t)\sqrt{2}U_{ph,nom} \quad (62)$$

$$U_{ph,nom} = \frac{U_{LL,nom}}{\sqrt{3}} \quad (63)$$

where U_{pk} – is peak phase voltage amplitude, V; $U_{ph,nom}$ – is nominal per-phase RMS voltage, V; $U_{LL,nom}$ – is nominal line-to-line RMS voltage, V.

αβ flux–current dynamics. Rotor flux dynamics:

$$\psi_{ra}^{\bullet} = \frac{L_m}{\tau_r} i_{s\alpha} - \frac{1}{\tau_r}\psi_{r\alpha} - \omega_{r,e}\psi_{r\beta} \quad (64)$$

$$\psi_{r\beta} = \frac{L_m}{\tau_r} i_{s\beta} - \frac{1}{\tau_r}\psi_{r\beta} + \omega_{r,e}\psi_{r\alpha} \quad (65)$$

Stator current dynamics:

$$i_{s\alpha}^{\bullet} = \frac{1}{\sigma L_s}(\nu_{s\alpha} - R_1 i_{s\alpha} - k\psi_{r\alpha}^{\bullet}) \quad (66)$$

$$i_{s\beta}^{\bullet} = \frac{1}{\sigma L_s}(\nu_{s\beta} - R_1 i_{s\beta} - k\psi_{r\beta}^{\bullet}) \quad (67)$$

$$k = \frac{L_m}{L_r} \quad (68)$$

Electromagnetic torque:

$$T_e = \frac{3}{2} 2p \frac{L_m}{L_r}(\psi_{r\alpha} i_{s\beta} - \psi_{r\beta} i_{s\alpha}) \quad (69)$$

where T_e – is electromagnetic torque, Nm.

Mechanical equation:

$$J\omega_m = T_e - T_L - B\omega_m \quad (70)$$

where J – is inertia, kgm^2; B - is viscous friction coefficient, Nms/rad.

$$B \approx \frac{P_{f\omega}}{\omega_{m,rated}^2} \quad (71)$$

where $\omega_{m,rated}$ – is rated mechanical speed, rad/s.

Dataset construction for SINDYc. The simulated dataset stores:

$$x(t) = \left[i_{s\alpha}(t), i_{s\beta}(t), \psi_{r\alpha}(t), \psi_{r\beta}(t), \omega_m(t)\right] \quad (72)$$

$$u(t) = \left[\nu_{s\alpha}(t), \nu_{s\beta}(t), T_L(t)\right] \quad (73)$$

where x - contains state trajectories; u - contains input trajectories.

Time step:

$$\Delta t = t_{k+1} - t_k \quad (74)$$

Numerical derivatives:

$$\dot{X} \approx \nabla_t X \quad (75)$$

where X – is the stacked state matrix; $\dot{X}$ – is stacked derivative matrix.

Train/test split and normalization. A time split at index k_s defines training and test sets:

$$X_{train} = X[0 : k_s] \quad (76)$$

$$X_{test} = X[k_s : N] \quad (77)$$

$$U_{train} = U[0 : k_s] \quad (78)$$

$$U_{test} = U[k_s : N] \quad (79)$$

where N – is the number of samples; k_s – is split index.

Z-score normalization:

$$X_n = \frac{X - \mu_x}{\sigma_X} \quad (80)$$

$$U_n = \frac{U - \mu_U}{\sigma_U} \quad (81)$$

where μ_x, μ_U – are per-component means; σ_X, σ_U – are per-component standard deviations.

Derivative scaling follows:

$$\dot{X}_n = \frac{\dot{X}}{\sigma_X} \quad (82)$$

SINDYc formulation. SINDYc seeks a sparse model of the form:

$$\dot{x}_n(t) = \theta(x_n(t), u_n(t))\Xi \quad (83)$$

where x_n – is normalized state vector; u_n – is normalized input vector; θ – is a library of candidate nonlinear features; Ξ – is a sparse coefficient matrix.

Feature library is a polynomial library up to degree 2:

$$\theta = \left[1, x_i, u_j, x_i x_k, x_i u_j, u_j u_i, ...\right] \quad (84)$$

where x_i – are components of x_n; u_j – are components of u_n.

Sparse regression uses Sequential Thresholded Least Squares (STLSQ).

Model simulation and error metrics. To evaluate generalization, the identified SINDYc model is simulated on the test interval using a fixed-step RK4 scheme:

$$x_n[k+1]=x_n[k]+\frac{h}{6}(k_1+2k_2+2k_3+k_4) \quad (85)$$

where h – Δt is step size, s; $k_1,...,k_4$ - are RK4 stage derivatives:

$$\dot{x}_n = f(x_n,u_n) \quad (86)$$

RMSE per state:

$$RMSE_n^{(i)}=\sqrt{\frac{1}{N}\sum_{k=1}^{N}\left(x_{n,i}^{pred}[k]-x_{n,i}^{true}[k]^2\right)} \quad (87)$$

Physical-unit reconstruction:

$$x_i^{pred}=x_{n,i}^{pred}\sigma X,i+\mu X,i \quad (88)$$

where x_i^{pred} – has the physical units of state i.

RMSE in physical units:

$$RMSE^{(i)}=\sqrt{\frac{1}{N}\sum_{k=1}^{N}\left(x_i^{pred}[k]-x_i^{true}[k]^2\right)} \quad (89)$$

Sparsity sweeps and final model selection. A set of thresholds $\lambda\in\{\lambda_1,...,\lambda_M\}$ is evaluated. For each λ the model computes:

$$N_{terms}(\lambda)=\#\{|\xi|>0\} \quad (90)$$

$$\overline{RMSE_n}(\lambda)=\frac{1}{n_x}\sum_{i=1}^{n_x}RSME_n^{(i)}(\lambda) \quad (91)$$

where n_x – is number of states.

A Pareto-style selection is applied: choose the simplest model whose error is within a tolerance of the best:

$$\overline{RMSE_n}(\lambda)\le(1+\delta)_\lambda^{\min}\overline{RMSE_n}(\lambda) \quad (92)$$

where δ – is allowable degradation.

RESULTS AND DISCUSSION

Based on the results of identification from no-load and locked-rotor tests, the following estimates of the parameters of the equivalent circuit were obtained for the Y connection: $R_c=143.833$ Ohm, $X_m=123.923$ Ohm, $R_{eq}=3.148$ Ohm, $X_{eq}=9.661$ Ohm, $Z_{sc}=10.161$ Ohm. For the locked-rotor mode, after filtering by the physically correct power factor, only two valid points were used, which reduces the stability of R_{eq}, X_{eq} and, as expected, increases the uncertainty of comparing the locked-rotor curves. Selection of the closest catalog analogue by features $[R_c, X_m, R_{eq}, X_{eq}]$ and additional verification of the consistency of the curves gave the best candidate 3.0 kW, 400 V, 2904 rpm, 2 poles, $\eta\approx87.1\%$, $j=0.0069$ kgm^2, Moreover, the gap from the second candidate according to the distance metric is about 28% ($ratio\approx1.28$), that is, the choice is justified, but not absolutely unambiguous. For the selected candidate, the inverse parameter estimation gave $R_1\approx R_2^{'}=1.400$ Ohm, $X_1\approx X_2^{'}=3.9410$ Ohm, $X_m=151.084$ Ohm, $R_c=876.144$ Ohm, $P_{mech}=55.81$ W. The derived dynamical parameters correspond to a physically plausible small scattering coefficient $\sigma\approx0.05$ and consistent time constants $T_s\approx T_r\approx0.352$ s, which is a consequence of the close symmetry of the pairs $R_1/R_2^{'}$ and L_s/L_r.

Comparison of experimental and calculated static characteristics showed that the no-load current at low voltages is reproduced satisfactorily, however, in the zone of large U_{LL} the model systematically underestimates I_o, which is consistent with the fact that the linear magnetic branch does not reflect the increase in the magnetizing current when approaching the nominal modes, Figure 1.

The active no-load power in the entire voltage range is overestimated relative to measurements, and the discrepancy increases with voltage, which indicates a mismatch in the level of losses in the magnetic branch and/or the accepted representation of mechanical/additional losses for the selected catalog analogue, Figure 2.

For the locked-rotor mode, current and power reproduce the general trend with voltage, but there is a transition from underestimation at the lower point to overestimation at the upper point, which is expected given the small number of valid experimental short-circuit points and the use of a constant parametric model without taking into account the change in equivalent resistances/reactivities in the locked-rotor mode Figure 3 and Figure 4.

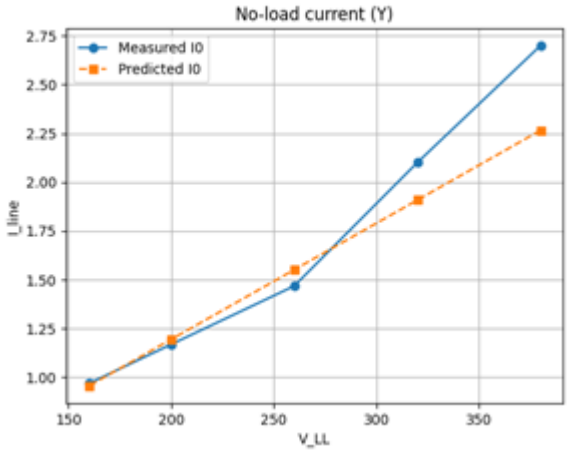

Fig. 1. Dependence of line current on line voltage in the no-load experiment of a three-phase asynchronous electric motor.

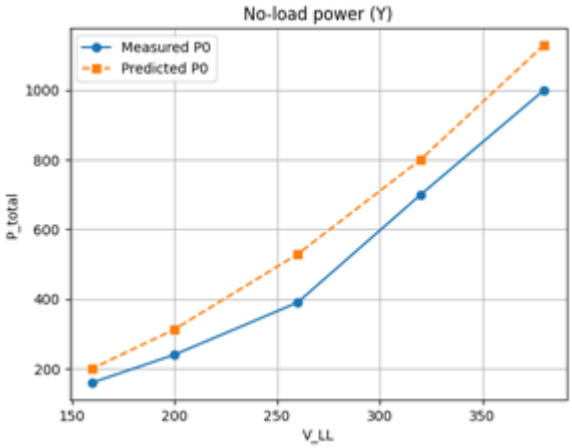

Fig. 2. Dependence of active power on line voltage in the no-load experiment of a three-phase asynchronous electric motor.

In general, the obtained results confirm the correctness of the identification of the motor class (2-pole, about 3 kW) and the suitability of the selected parameters as starting ones for further construction of a dynamic model and synthetic dataset for SINDYc, while the most significant inconsistencies are concentrated in the reproduction of no-load losses and in the accuracy of locked-rotor curves at upper voltages.

The next step was to obtain a dataset for SINDYc based on a dynamic model of an asynchronous motor in the αβ-coordinate system. The generated dataset has a size of 4001x14, which corresponds to modeling at an interval of 2.0 s with a sampling step of 0.0005 s and contains the full set of values required for SINDYc: time *t*, states $i_\alpha, i_\beta, \psi_{r,\alpha}, \psi_{r,\beta}, \omega_m$, control influences ν_α, ν_β and T_{Load}, as well as state derivatives calculated numerically with a consistent length of series.

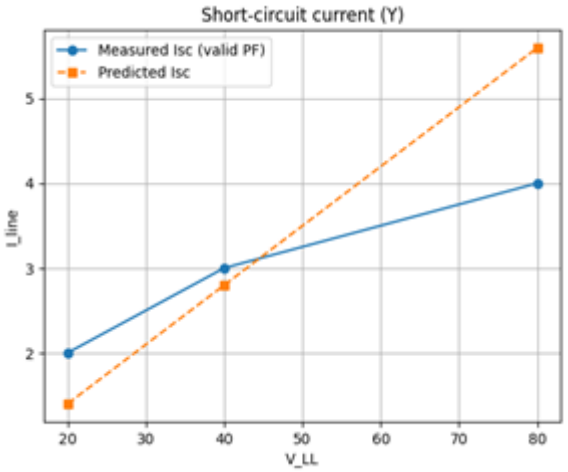

Fig. 3. Dependence of line current on line voltage in a short-circuit experiment of a three-phase asynchronous electric motor.

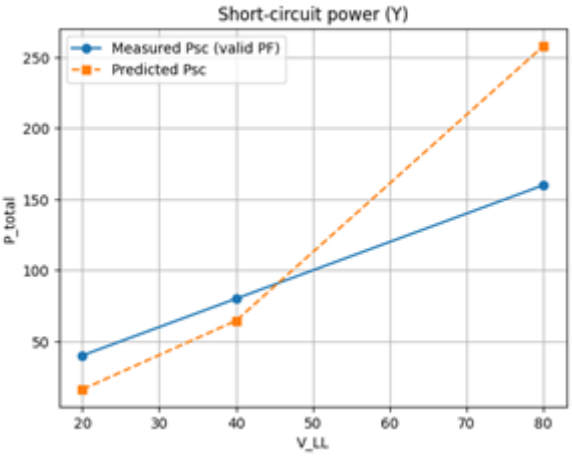

Fig. 4. Dependence of active power on line voltage in a short-circuit experiment of a three-phase asynchronous electric motor.

The initial rows of the dataset demonstrate the correct startup transient: at the moment t = 0 all states are equal to zero, then against the background of a smooth increase in voltages ν_α, ν_β small currents and flows appear, and the mechanical speed in the early steps remains practically zero. This is expected, because the electromagnetic moment is still being formed, and the rotor inertia does not allow the speed to change instantly. The values of the derivatives at the start are finite and grow together with the excitation amplitude, which indicates the absence of numerical instability or discontinuities in the control profiles. It is especially important that T_{Load} is zero at the beginning, i.e. the first segment of the data reflects the acceleration mode

without load, after which (according to the profile) the data contain several step changes in the load moment. This creates informative disturbances for identification and increases the observability of the connection between the electrical states and the mechanical subsystem. As a result, the structure of the dataset is correct for SINDYc: there are both states, and controls, and their consistent derivatives with the same time step, and the numerical values themselves at the start and the nature of the transition correspond to the physics of the process, i.e. the data can be considered adequate for further sparse reconstruction of the equations of motion.

The state matrix X_{SINDY} has size (4001, 5), i.e. it contains 4001 time counts of the five states of the model $i_\alpha, i_\beta, \psi_{r,\alpha}, \psi_{r,\beta}, \omega_m$. The control influence matrix U_{SINDY} has the size (4001, 3) and corresponds to the same 4001 samples for the three inputs ν_α, ν_β and T_{Load}. The state derivative matrix X_{SINDY} also has size (4001.5), which means there is no shift in lengths between X, U, $\dot{X}$. A critically important condition for the correct solution of the regression problem in SINDYc, since each state time reference corresponds to the same control and derivative time reference.

The sampling step $DT_{SINDTY} = 0.5$ ms provides high time resolution for electromagnetic processes in the αβ system, where variables can have rapid oscillations at the power frequency. Such discretization reduces the error of numerical differentiation when calculating X and improves the quality of subsequent reconstruction of equations, especially for terms containing the interaction of electrical and mechanical variables.

Such discretization reduces the error of numerical differentiation when calculating $\dot{X}$ and improves the quality of subsequent reconstruction of equations, especially for terms containing the interaction of electrical and mechanical variables.

The simulation time graphs in αβ-coordinates demonstrate physically plausible drive dynamics with given profiles, Figure 5-7.

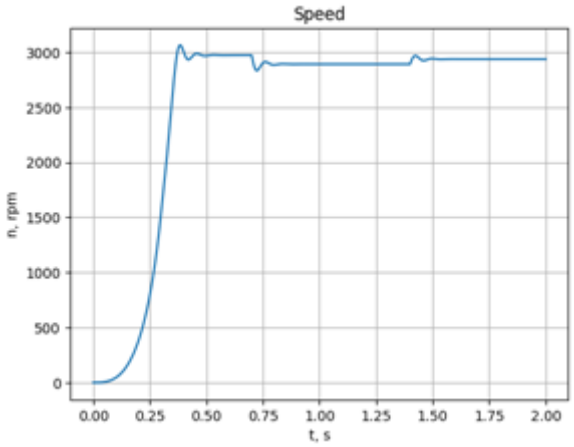

Fig. 5. Dependence of setting the nominal rotor speed of a three-phase asynchronous electric motor in the transient mode.

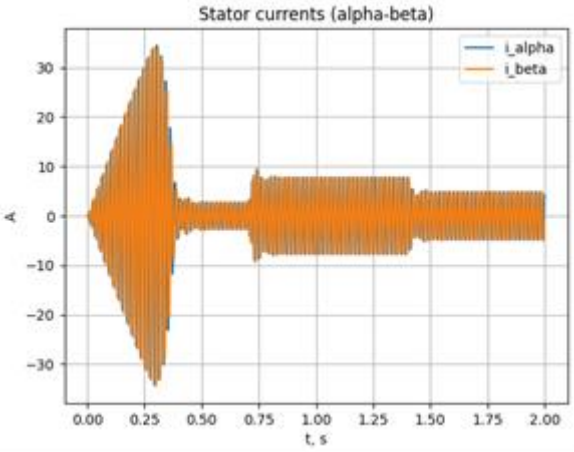

Fig. 6. Dependence of the change in the stator current of a three-phase electric motor in the transient mode (starting mode).

The speed increases from zero to the near-synchronous region (3000 rpm) in approximately 0.3-0.4 s with a slight overshoot and subsequent settling. This corresponds to the acceleration of an asynchronous motor as the voltage increases. Stator currents i_α and i_β have the largest amplitude during start-up (typical starting current), after which they decrease in steady state, and with step changes in load, corresponding changes in amplitude are visible. On the moment graph, the electromagnetic moment T_e qualitatively fulfills the specified profile T_{Load}. At each load jump, a transient process with short-term peaks/oscillations occurs, after which T_e coincides with the load level in the steady state. After a load decrease of about 1.4 s, a decline and

a short transient process T_e are observed, which is also expected.

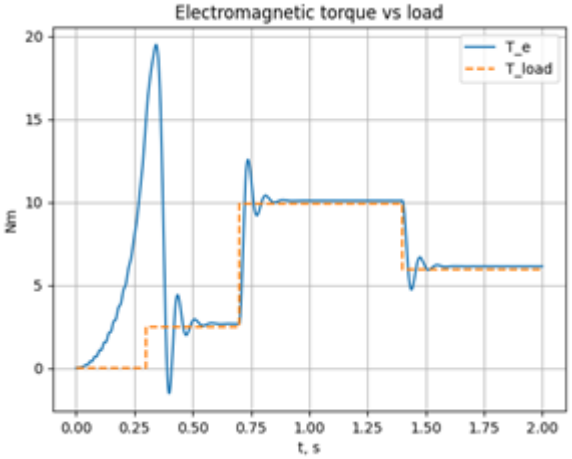

Fig. 7. Dependence of the change in the electromagnetic torque of a three-phase electric motor in the transient mode (starting mode) in the mode of step change in load.

The next step was to split the sample. The training part contains 2000 samples (0–1.0 s), the test part contains 2001 samples (1.0–2.0 s). Since the sampling step is 0.0005 s, 2000 points correspond to exactly 1 second of data, and the test part retains the same sampling frequency and full dimensionality consistency between the states *X*, the inputs *U*, and the derivatives $\dot{X}$. This division ensures that the model is trained on the transient acceleration mode and the first part of the load response, and tested on the following modes after 1.0 s, where other operating areas and load changes are present. This is important for assessing the generalization ability of SINDYc: the model will not simply repeat the trajectory from training, but must reproduce the dynamics on the time interval that was not used in the fitting.

Next, normalization was performed. After scaling, the dimensions of the arrays did not change: the full set has 4001 counts for the states $X \in R^{4001x5}$, inputs $X \in R^{4001x3}$ and derivatives $X \in R^{4001x5}$. Similarly, 2000 samples were stored for the training part, and 2001 for the test part.

In the test validation of the identified SINDYc model, a stable numerical simulation was obtained over the entire test interval (all trajectories are finite, without divergence), which indicates the suitability of the found system of equations as a predictive approximation of dynamics. The reproduction errors are estimated via RMSE both in the normalized state space and after returning to physical units. In the normalized form, the error for the stator currents is about 0.079 for i_α and i_β, for the rotor flux linkages about 0.037 for $\psi_{r,\alpha}$ and $\psi_{r,\beta}$, and for the mechanical angular velocity 0.0247, which indicates the best agreement for the mechanical channel and the rotor compared to the current channels. In physical units, the RMSE is approximately 0.81 A for i_α and i_β, about 0.0197 Wb for $\psi_{r,\alpha}$ and $\psi_{r,\beta}$, and 3.09 rad/s for ω_m, which is equivalent to approximately 30 rpm. Thus, the model most accurately reproduces the speed and rotor fluxes, while the error for currents is larger, which is typical for derivative-based identification and can be attributed to the high-frequency component of the signals and the sensitivity of RMSE to phase shifts in the oscillatory components.

After automatic detection of load change moments, the test section was divided into two time segments: the first from t=1.0 s to t≈1.399 s (800 counts), the second from t=1.4 s to t=2.0 s (1201 counts). This division corresponds to the jump point of the load moment control signal, i.e., the change in the operating mode of the electric drive. The estimation of the model error separately for each segment showed the expected degradation of accuracy after the load jump. In segment 0, the average normalized RMSE for all states is 0.039, with the smallest errors observed for the mechanical speed ω_m (0.0216) and the rotor flux linkages $\psi_{r,\alpha}$ and $\psi_{r,\beta}$ (0.027), while for the currents i_α and i_β the error is about 0.06. In segment 1, the average normalized RMSE increases to 0.058, and the errors for the currents increase to 0.0893, for the flux linkages to 0.0423, and for the speed to 0.0265.

The results of the sparsity sweep of the SINDYc model showed that in the studied range of STLSQ thresholds, the accuracy on the test sample almost does not change, while the number of active terms in the equations changes moderately. For most threshold values in the interval 0.01–0.50, almost the same average error level was obtained: 0.047808, while the model contains about 225 non-zero terms. This means that in this range, regularization is not a limiting factor: the structure of the feature library and the data lead to almost the same solution, and changing the threshold does not affect the consistency of the model with the test dynamics. Increasing the threshold to 0.80 gave the lowest

average error among the tested options (0.047772) at 223 terms. At the same time, further increasing the sparsity to 1.20 reduced the model complexity to 216 terms, but led to a slight deterioration in accuracy (0.047843). The difference in error between these models is very small (on the order of 10^{-4}), indicating actual equivalence in accuracy at different levels of complexity.

According to the results of sparsity selection, the final model was selected according to the rule almost the best accuracy + minimum complexity. Then, an allowable deterioration in accuracy of 3% was set, so the threshold value was 0.0492048. Among all the models that fell into this quality corridor, the option with the smallest number of active members was selected: threshold 1.2, 216 non-zero terms, while the average error remained practically at the optimum level. This means that a small fee in accuracy (compared to the absolute minimum) is compensated by a noticeably simpler structure of the equations, which increases interpretability and reduces the risk of overtraining without losing the adequacy of reproducing the test dynamics.

In the test interval (t = 1.0–2.0 s), the final SINDYc model after selection according to the criterion 3% of the best RMSE + minimum terms (threshold 1.2, 216 active members) demonstrate stable reproduction of the dynamics of all five states in the normalized space and in physical units. According to the integral error estimate, the RMSE (normalized) for the currents i_α and i_β was obtained at the level of 0.0734, for the rotor flux linkages $\psi_{r,\alpha}$ and $\psi_{r,\beta}$ about 0.0343, and for the mechanical angular velocity ω_m 0.0237. In physical units, this corresponds to RMSE 0.754 A for each current component, 0.01827 (in your units for flux linkage used in the model) for the rotor flux linkage components, and 2.97 rad/s for ω_m. This distribution of errors is expected: the speed as a slow state is reproduced more accurately, while the currents are more sensitive to non-smooth load changes and contain a pronounced oscillatory component at the supply frequency.

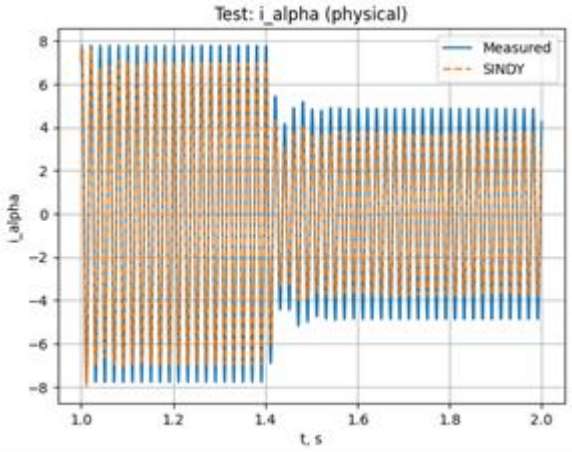

Fig. 8. Dependence of the change in the stator current of a three-phase electric motor in the transient mode (starting mode) in the α coordinates.

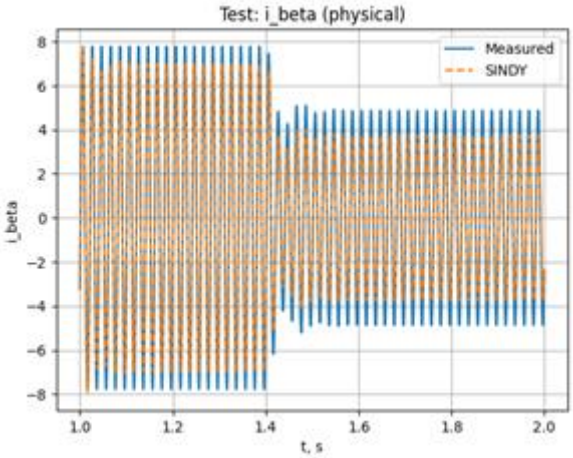

Fig. 9. Dependence of the change in the stator current of a three-phase electric motor in the transient mode (starting mode) in the β coordinates.

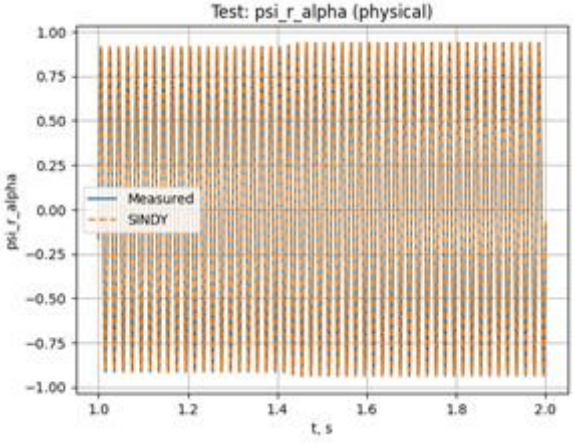

Fig. 10. Dependence of the change in the value of the flux linkage of the rotor of a three-phase electric motor in the transient mode (starting mode) in the α coordinates.

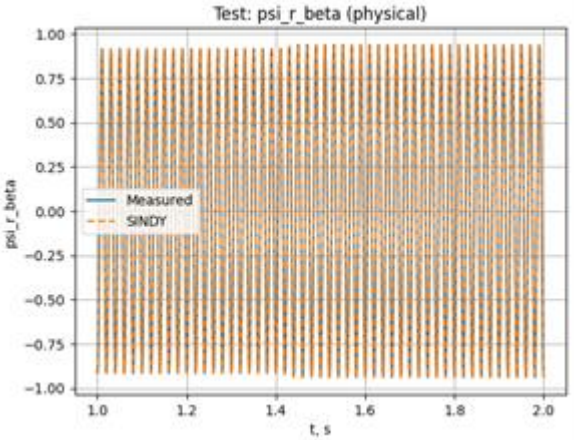

Fig. 11. Dependence of the change in the value of the flux linkage of the rotor of a three-phase electric motor in the transient mode (starting mode) in the β coordinates.

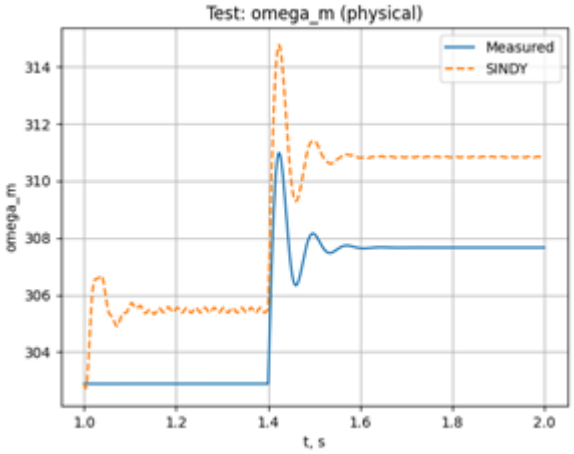

Fig. 12. Dependence of the change in the angular frequency of the rotor of a three-phase electric motor in the transient mode (starting mode).

Figure 8-12, comparison on the test interval shows that the SINDYc model well reproduces the phase and amplitude of fast vibration components for $i_\alpha, i_\beta, \psi_{r,\alpha}, \psi_{r,\beta}$, and adequately reproduces the response to a change in load at a time of about t = 1.4 s. The most noticeable systematic discrepancy is manifested precisely in the speed: after a load jump, SINDYc reproduces the correct transient behavior (overshoot and damping), but exhibits a shift of the steady-state level ω_m relative to the measured trajectory. This behavior is consistent with the fact that the mechanical channel is integrating and sensitive to small errors in the reproduction of torque and losses (friction/load); even a small error in the model of the interconnection of currents and flux linkages leads to the accumulation of a difference in speed, so it is ω_m that is often the most demanding variable for data-driven identification.

CONCLUSIONS

The article studies the dynamic behavior of induction motors and estimates key electromechanical parameters using the SINDYc method in conditions where only the results of no-load and short-circuit tests and a dataset with reference data of various three-phase induction motors of the AIR series are available.

The work obtained the parameters of the equivalent circuit from no-load and short-circuit, which became the basis for building mechanical and electrical models of the motor. The dynamics of signals (currents, voltages, torque, unbalanced magnetic force) was calculated based on the mechanical model of rotor acceleration and electrical variables agreed with it. The SINDYc model was built and trained. During the verification of the validity of the identified SINDYc model, a stable numerical simulation was obtained over the entire test interval (all trajectories are finite, without divergence), which indicates the suitability of the found system of equations as a predictive approximation of dynamics. Reproduction errors are estimated with the help of RMSE both in the normalized state space and after returning to physical units. In the normalized form, the error for the stator currents is about 0.079, for the flux-coupled rotor about 0.037, and for the mechanical angular velocity 0.0247, which indicates the best correspondence for the mechanical channel and the rotor compared to the current channels. The results of the analysis of the sparseness of the SINDYc model showed that in the studied range of STLSQ threshold values, the accuracy on the test sample practically does not change, while the number of active terms in the equations changes moderately. For most of the threshold values in the interval 0.01–0.5, an almost identical average error level was obtained: 0.047808, while the model contains about 225 non-zero terms. An assessment of the change in the stator current and the value of the rotor flux linkage of a three-phase electric motor in the transient mode (starting mode) in the coordinates α and β was carried out. As a result of the conducted research, it was found that the SINDYc method is advisable to use for predicting key electromechanical parameters of electric motors in the absence of information on the nature of power loads, which is typical for mixing

systems in biogas plants and other technological processes.

REFERENCES

[1] Barrera-Llanga, K., Burriel-Valencia, J., Sapena-Bano, A., Martinez-Roman, J. (2025) "Fault detection in induction machines using learning models and fourier spectrum image analysis," *Sensors*, vol. 25, no. 2, 471 p.

[2] Konuhova, M. (2025). "Induction Motor Dynamics Regimes: A Comprehensive study of Mathematical Models and Validation," *Applied Sciences*, vol. 15, no. 3, 1527 p.

[3] Deublein, D., Steinhauser, A. (2008). Biogas from Waste and Renewable Resources. An Introduction. KGaA, Weinheim, 450 p.

[4] Ward, A. J., Hobbs, P. J., Holliman, P. J., & Jones D. L. (2008). Optimisation of the anaerobic digestion of agricultural resources. *Bioresource Technology*, 99, pp. 7928-7940.

[5] Latha, K., Velraj, R., Shanmugam, P. & Sivanesan, S. (2019). Mixing strategies of high solids anaerobic co-digestion using food waste with sewage sludge for enhanced biogas production. *Journal of Cleaner Production*, 210, pp. 388–400.

[6] Foukrach, M., Bouzit, M., & Ameur, H. (2020). Effect of Agitator's Types on the Hydrodynamic Flow in an Agitated Tank. *Chinese Journal of Mechanical Engineering*. 33. 37 p.

[7] Ameur, H. (2016). Mixing of complex fluids with flat and pitched bladed impellers: effect of blade attack angle and shear-thinning behavior. *Food and Bioproducts Processing*, 99, pp. 71-77.

[8] Marks, S., Dach, J., Fernandez, M. F. J., Mazurkiewicz, J., Pochwatka, P., & Gierz, Ł. (2020). New Trends in Substrates and Biogas Systems in Poland. *Journal of Ecological Engineering*, 21(4), pp. 19-25.

[9] Lunyaka, K. V., Vus, D. N., Rusanov, S. A., & Klyuev, O. I. (2009). Dissolution of solids with stirring with stirrers in vessels with vertical partitions. *Theory and practice of modern natural science*. 36-39.

[10] Zakomorny, D. M., Povodzinsky, V. M., & Shibetsky, V. Yu. (2015). Classification and analysis of fermenters with mechanical mixing devices in aerobic processes of biotechnology. *ScienceRise*, 5(2), pp. 24-32.

[11] Boldea, I. (2020). Induction Machines Handbook: Transients, Control Principles, Design and Testing; *CRC Press: Boca Raton*, FL, USA.

[12] Gundewar, S.K.; Kane, P.V. (2021) Condition monitoring and fault diagnosis of induction motor. *J. Vib. Eng. Technol*. Vol. 9, pp. 643–674.

[13] Terron-Santiago, C.; Martinez-Roman, J.; Puche-Panadero, R.; Sapena-Bano, A. (2021). A review of techniques used for induction machine fault modelling. *Sensors*, vol. 21, pp. 48-55.

[14] Swana, E.F.; Doorsamy, W.; Bokoro, P. (2022). Tomek link and SMOTE approaches for machine fault classification with an imbalanced dataset. *Sensors*, vol. 22, pp. 32-46.

[15] Orlowska-Kowalska, T.; Wolkiewicz, M.; Pietrzak, P.; Skowron, M.; Ewert, P.; Tarchala, G.; Krzysztofiak, M.; Kowalski, C.T. (2022). Fault diagnosis and fault-tolerant control of PMSM drives–state of the art and future challenges. *IEEE Access*, vol. 10, 59979–60024.

[16] Toma, R.N.; Prosvirin, A.E.; Kim, J.M. (2020). Bearing fault diagnosis of induction motors using a genetic algorithm and machine learning classifiers. *Sensors*, 20, 1884.

[17] Gangsar, P.; Tiwari, R. (2020). Signal based condition monitoring techniques for fault detection and diagnosis of induction motors: A state-of-the-art review. *Mech. Syst. Signal Process.*, 144, 106908.

[18] Singh, M.; Shaik, A.G. (2020). Incipient fault detection in stator windings of an induction motor using stockwell transform and SVM. *IEEE Trans. Instrum. Meas*, 69, 9496–9504.

[19] L. Huang, G. Shen, N. Hu, L. Chen, and Y. Yang, (2022). "Coupled Electromagnetic-Dynamic Modeling and Bearing Fault Characteristics of Induction Motors considering Unbalanced Magnetic Pull," *Entropy*, vol. 24, no. 10, p. 1386.

[20] B. Wang, C. Lin, H. Inoue, and M. Kanemaru, (2022). "Topological data analysis for electric motor eccentricity fault detection," *in IECON 2022 – 48th Annual Conference of the IEEE Industrial Electronics Society*, pp. 1–6.

[21] E. Vancayseele, P. Desenfans, Z. Gong, D. Vanoost, H. De Gersem, and D. Pissoort, (2025). "Data-Driven Model Identification of Unbalanced Induction Motor Dynamics and Forces using SINDYc,".

[22] Sapena-Bañó, A.; Martinez-Roman, J.; Puche-Panadero, R.; Pineda-Sanchez, M.; Perez-Cruz, J.; Riera-Guasp, M. (2018). Induction machine model with space harmonics for fault diagnosis based on the convolution theorem. *Int. J. Electr. Power Energy Syst.*, 100, pp. 463–481.

[23] Burriel-Valencia, J.; Puche-Panadero, R.; Martinez-Roman, J.; Sapena-Bañó, A.; Pineda-Sanchez, M. (2017). Short-frequency Fourier transform for fault diagnosis of induction machines working in transient regime. *IEEE Trans. Instrum. Meas.*, 66, pp. 432–440.

[24] Singh, M.; Shaik, A.G (2020). Incipient fault detection in stator windings of an induction motor using stockwell transform and SVM. *IEEE Trans. Instrum. Meas*., 69, pp. 9496–9504.

[25] Kaparthi, S.; Bumblauskas, D. (2020). Designing predictive maintenance systems using decision tree-based machine learning techniques. *Int. J. Qual. Reliab. Manag*., 37, pp. 659–686.

[26] Tran, M.Q.; Liu, M.K.; Tran, Q.V.; Nguyen, T.K. (2021). Effective fault diagnosis based on wavelet

and convolutional attention neural network for induction motors. *IEEE Trans. Instrum. Meas., 71*.
[27] Saxena, A.; Kumar, R.; Rawat, A.K.; Majid, M.; Singh, J.; Devakirubakaran, S.; Singh, G.K. (2023). Abnormal Health Monitoring and Assessment of a Three-Phase Induction Motor Using a Supervised CNN-RNN-Based Machine Learning Algorithm. *Math. Probl. Eng*.
[28] Li, Y.; Cao, J.; Xu, Y.; Zhu, L.; Dong, Z.Y. (2024). Deep learning based on Transformer architecture for power system short-term voltage stability assessment with class imbalance. *Renew. Sustain. Energy Rev., 189*.
[29] Al-Shorman, O.; Irfan, M.; Saad, N.; Zhen, D.; Haider, N.; Glowacz, A.; AlShorman, A. (2020). A review of artificial intelligence methods for condition monitoring and fault diagnosis of rolling element bearings for induction motor. *Shock Vib*.
[30] Glowacz, A. (2023). Thermographic fault diagnosis of electrical faults of commutator and induction motors. *Eng. Appl. Artif. Intell. 121*.
[31] Ngoc, H.V.; Mayer, J.; Bitar-Nehme, E. (2022). Deep learning LSTM for predicting thermally induced geometric errors using rotary axes' powers as input parameters. *CIRP J. Manuf. Sci. Technol., 37*, pp. 70–80.
[32] S. L. Brunton, J. L. Proctor, and J. N. Kutz, (2016). "Discovering governing equations from data by sparse identification of nonlinear dynamical systems," *Proceedings of the National Academy of Sciences*, vol. 113, no. 15, pp. 3932–3937.
[33] M. A. Abu-Seif (2023). "Data-Driven-Based vector space decomposition modeling of multiphase induction machines," *IEEE Transactions on Energy Conversion*, vol. 38, no. 3, pp. 2061–2074.
[34] Brunton, B.W., Johnson, L.A., Ojemann, J.G., and Kutz, J.N. (2016). Extracting spatial-temporal coherent patterns in largescale neural recordings using dynamic mode decomposition. *Journal of Neuroscience Methods*, 258, pp. 1–15.
[35] Brunton, S.L. and Noack, B.R. (2015). Closed-loop turbulence control: Progress and challenges. *Applied Mechanics Reviews*, 67.
[36] Brunton, S. L., Proctor, J. L. & Kutz, J. N. (2016). Sparse identification of nonlinear dynamics with control (SINDYc). *IFAC NOLCOS* 49 (18), pp. 710–715
[37] Ayankoso, S., Olejnik, P., (2023). "Time-Series Machine Learning Techniques for Modeling and Identification of Mechatronic Systems with Friction: A Review and Real Application," *Electronics*, vol. 12, no. 17, p. 3669.
[38] Motamedi, Fahimeh; Sanchez, Horacio; Mehri, Alireza; Ghasemi, Fahimeh (2021). "Accelerating Big Data Analysis through LASSO-Random Forest Algorithm in QSAR Studies". *Bioinformatics*. 37, pp. 469–475.

Information about authors.

Spodoba Mykhailo Oleksiiovych. Doctor of Philosophy (Ph.D). Main area of research: Energy efficiency of technological processes of production, light and heavy industry.
E-mail: spmisha@ukr.net
ORCID: https://orcid.org/0000-0001-6179-0825

Spodoba Oleksandr Oleksiiovych. Doctor of Philosophy (Ph.D). Main area of research: Energy efficiency of hydraulic drives.
E-mail: sp1309@ukr.net
ORCID: https://orcid.org/0000-0001-8217-866X

Kovalchuk Stanislav Igorovich. Doctor of Philosophy (Ph.D). Main area of research: Electrical engineering.
E-mail: stas_kovalchuk@outlook.com
ORCID: https://orcid.org/0000-0002-1194-3464